RCS analysis of canonical, two-dimensional material-loaded cavities with rectangular and circular cross sections

Kazuya KOBAYASHI *
Alexander I. NOSICH **

Abstract

A rigorous radar cross section (RCS) *analysis of canonical, two-dimensional material-loaded cavities with rectangular and circular cross sections is carried out using the Wiener-Hopf technique and the Riemann-Hilbert problem technique, respectively. Both E and H polarizations are treated. It is shown via numerical examples that the absorbing layer loading inside the cavities gives rise to the significant* RCS *reduction. The results can be used as a reference solution for validating more general-purpose computer codes based on approximate methods.*

Key words : Cross section, Radar target, Bidimensional model, Canonical form, Rectangular configuration, Circular configuration, Wave diffraction, Wiener Hopf method, Cavity.

ANALYSE EN SER DE CAVITÉS CANONIQUES À DEUX DIMENSIONS CHARGÉES EN MATÉRIAUX ET COMPORTANT DES SECTIONS RECTANGULAIRES OU CIRCULAIRES

Résumé

L'analyse rigoureuse de la détermination de la surface équivalente radar de cavités canoniques 2-D chargées d'un matériau, ayant une section rectangulaire ou circulaire par les méthodes de Wiener-Hopf et de Riemann-Hilbert, les polarisations E et H sont traitées. A partir d'exemples numériques, on montre que la couche de matériau chargeant les cavités entraîne une réduction significative de la SER. *Ces résultats peuvent être utilisés comme références de calcul pour valider des programmes basés sur des méthodes approchées.*

Mots clés : Section efficace, Cible radar, Modèle bidimensionnel, Forme canonique, Configuration rectangulaire, Configuration circulaire, Diffraction onde, Méthode Wiener Hopf, Cavité.

Contents

I. *Introduction.*
II. *A cavity with rectangular cross section : the Wiener-Hopf approach.*
III. *A cavity with circular cross section : the Riemann-Hilbert problem approach.*
IV. *Numerical results and discussion.*
References (15 ref.).

I. INTRODUCTION

Analysis of the scattering from open cavities is an important subject in target identification problems since these scatterers contribute significantly to the radar cross section (RCS) due to the interior irradiation. A number of investigations on the scattering from two-dimensional (2-D) and three-dimensional (3-D) cavities have been carried out thus far using the high-frequency (HF) asymptotic techniques and the moment method (MM) [1-7]. However, it appears that the solutions deduced *via* these methods are not uniformly valid for arbitrary cavity dimensions.

The Wiener-Hopf (WH) technique [8] and the Riemann-Hilbert problem (RHP) technique [9, 10] are

* Department of Electrical and Electronic Engineering, Chuo University, 1-13-27 Kasuga, Bunkyo-ku, Tokyo 112, Japan.
** Institute of Radiophysics and Electronics, Ukrainian Academy of Sciences, 12 Proskura st., Kharkov 310085, Ukraine.

powerful, rigorous approaches for solving diffraction problems associated with canonical geometries. There are some recent contributions on the scattering by cavities based on the WH and RHP techniques [11-14], in which accurate and reliable results are obtained over broad frequency range. In the present paper, we shall consider 2D rectangular and circular loaded cavities as related to the geometries in [13, 14], and analyze the plane wave diffraction for both E and H polarizations using the WH and RHP techniques, respectively. It is shown *via* illustrative numerical examples on the monostatic and bistatic RCS that the interior irradiation is significantly reduced for loaded cavities. In the following, the analysis procedure is presented only for the E-polarized case, but numerical results are given for both polarizations.

The time dependence $e^{-i\omega t}$ is suppressed throughout this paper.

II. A CAVITY WITH RECTANGULAR CROSS SECTION : THE WIENER-HOPF APPROACH

We consider a 2-D loaded cavity illuminated by an E-polarized plane wave, as shown in Figure 1, where the cavity plates are infinitely thin, perfectly conducting, and the material layer is characterized by the relative permittivity and permeability ε_r, μ_r. Let the total electric field be :

(1) $$E_z^t(x,y) = E_z^i(x,y) + E_z(x,y),$$

where $E_z^i(x,y)$ is the incident field defined by :

(2) $$E_z^i(x,y) = e^{-ik(x\cos\varphi_0 + y\sin\varphi_0)}, \quad 0 \le \varphi_0 \le \pi$$

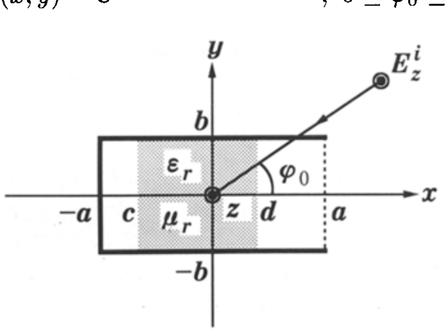

FIG. 1. — Geometry of the rectangular cavity.

Géométrie de la cavité rectangulaire.

with $k(=\omega\sqrt{\mu_0\varepsilon_0})$ being the free-space wavenumber. For convenience of analysis, we introduce a slight loss into the medium as in $k = k_1 + ik_2$ with $0 < k_2 \ll k_1$, and take the limit $k_2 \to +0$ at the end of analysis.

Let us define the Fourier transform of the scattered field $E_z(x,y)$ by :

(3)
$$\Phi(s,y) = \frac{1}{\sqrt{2\pi}}\int_{-\infty}^{\infty} E_z(x,y)e^{isx}\,dx, \quad s = \sigma + i\tau,$$

being regular in $|\tau| < k_2$. Taking the Fourier transform of the Helmholtz equation and solving the resultant equations, we may derive the scattered field representation in the complex domain. The field for $y \gtrless \pm b$ is given by :

(4) $$\Phi(s,y) = (1/2)\{e^{-isa}[U_-(s) \pm V_-(s)] + e^{isa}[U_+(s) \pm V_+(s)]\}e^{\mp\kappa(s)(y\mp b)},$$

where $\kappa(s) = \sqrt{s^2 - k^2}$ with Re $\kappa(s) > 0$, and

(5) $$U_\pm(s) = \Psi_\pm(s,b) + \Psi_\pm(s,-b), \quad V_\pm(s) = \Psi_\pm(s,b) - \Psi_\pm(s,-b),$$

(6) $$\Psi_\pm(s,y) = \Phi_\pm(s,y) \mp \frac{A_{1,2}e^{-iky\sin\varphi_0}}{s - k\cos\varphi_0}, \quad A_{1,2} = \frac{e^{\mp ika\cos\varphi_0}}{\sqrt{2\pi}i},$$

(7) $$\Phi_\pm(s,y) = \pm\frac{1}{\sqrt{2\pi}}\int_{\pm a}^{\pm\infty} E_z(x,y)\, e^{is(x\mp a)}\,dx.$$

Applying boundary conditions at the cavity surface and the material interface, the problem is formulated in terms of the Wiener-Hopf equations satisfied by $U_\pm(s)$ and $V_\pm(s)$. These equations can be solved exactly in a formal sense leading to the following exact solution :

(8a) $$U_\pm(s) = M_\pm(s)\left[\mp\frac{A_{1,2}^u}{\sqrt{b}(s - k\cos\varphi_0)} + J_{1,2}^u(s) \pm \sqrt{b}F_\pm^u(s)\right],$$

(8b) $$V_\pm(s) = N_\pm(s)\left[\pm\frac{A_{1,2}^v}{\sqrt{b}(s - k\cos\varphi_0)} + J_{1,2}^v(s) \pm \sqrt{b}F_\pm^v(s)\right],$$

where $M_\pm(s)$ and $N_\pm(s)$ are the WH split functions [12, 13], and

(9) $$A_{1,2}^u = \frac{2\sqrt{b}A_{1,2}\cos(kb\sin\varphi_0)}{M_\pm(k\cos\varphi_0)}, \quad A_{1,2}^v = \frac{2i\sqrt{b}A_{1,2}\sin(kb\sin\varphi_0)}{N_\pm(k\cos\varphi_0)},$$

(10) $$\left.\begin{matrix} J_{1,2}^u(s) \\ J_{1,2}^v(s) \end{matrix}\right\} = \frac{1}{\pi i}\times \int_k^{k+i\infty} \frac{e^{2iwa}\kappa(w)}{w \pm s}\begin{Bmatrix} M_+(w)U_\mp(\mp w) \\ N_+(w)V_\mp(\mp w)\end{Bmatrix}dw,$$

$$(11)\quad F^u_\pm(s) = \sum_{n=2}^{\infty} \left\{ \begin{matrix} \chi_{2n-3} \\ 1 \end{matrix} \right\} \frac{f_n p_n u_n^\pm}{b(s \pm \mathrm{i}\kappa_{2n-3})},$$

$$F^v_\pm(s) = \sum_{n=2}^{\infty} \left\{ \begin{matrix} \chi_{2n-2} \\ 1 \end{matrix} \right\} \frac{g_n q_n v_n^\pm}{b(s \pm \mathrm{i}\kappa_{2n-2})},$$

$$(12)\quad \chi_n = \frac{\mathrm{e}^{-2\kappa_n(a-d)}\left[\sigma_n' \mathrm{e}^{-2K_n(d-c)} - \sigma_n\right]}{1 - \sigma_n' \sigma_n \mathrm{e}^{-2K_n(d-c)}},$$

$$(13)\quad \sigma_n = \frac{\mu_r \kappa_n - K_n}{\mu_r \kappa_n + K_n},$$

$$\sigma_n' = \frac{\mu_r \kappa_n - \tau_n K_n}{\mu_r \kappa_n + \tau_n K_n},\ \tau_n = \frac{1 - \mathrm{e}^{-2\kappa_n(c+a)}}{1 + \mathrm{e}^{-2\kappa_n(c+a)}},$$

(14)

$$f_n = [(n - 3/2)\pi]^2 / b\mathrm{i}\kappa_{2n-3},\ g_n = [(n-1)\pi]^2 / b\mathrm{i}\kappa_{2n-2},$$

$$(15)\quad p_n = M_+(\mathrm{i}\kappa_{2n-3})/\sqrt{b},\ q_n = N_+(\mathrm{i}\kappa_{2n-2})/\sqrt{b},$$

$$(16)\quad u_n^\pm = U_\pm(\pm \mathrm{i}\kappa_{2n-3})/b,\ v_n^\pm = V_\pm(\pm \mathrm{i}\kappa_{2n-2})/b,$$

$$(17)\quad \kappa_n = \sqrt{(n\pi/2b)^2 - k^2},$$

$$K_n = \sqrt{(n\pi/2b)^2 - k'^2},\ k' = \sqrt{\mu_r \varepsilon_r}k.$$

We may apply the method established in [12] to derive approximate formulas for the infinite series $F^u_\pm(s)$, $F^v_\pm(s)$ and the branch-cut integrals $J^u_{1,2}(s)$, $J^v_{1,2}(s)$ defined by (10) and (11). In particular, the asymptotic expansions of $J^u_{1,2}(s)$ for large $|k|a$ are found to be

$$(18)\quad J^u_{1,2}(s) \sim \sqrt{b} f_1 p_1 \left\{ \left[u_1^\mp + \frac{2A_{2,1}\cos(kb\sin\varphi_0)}{kb(1 \pm \cos\varphi_0)} \right] \times \xi(\pm s) + \frac{2aA_{2,1}}{b} \cos(kb\sin\varphi_0)\eta(\pm s, \pm k\cos\varphi_0) \right\},$$

and the approximate expressions of $F^u_\pm(s)$ are derived as :

$$(19)\quad F^u_\pm(s) \approx \sum_{n=2}^{N} \left\{ \begin{matrix} \chi_{2n-3} \\ 1 \end{matrix} \right\} \frac{f_n p_n u_n^\pm}{b(s \pm \mathrm{i}\kappa_{2n-3})} + C^u_{1,2} \sum_{n=N+1}^{\infty} \left\{ \begin{matrix} \chi_{2n-3} \\ 1 \end{matrix} \right\} \frac{f_n (b\kappa_{2n-3})^{-c_{1,2}}}{b(s \pm \mathrm{i}\kappa_{2n-3})},$$

for large N with $c_1 = 2 (d \neq a)$; $= 3/2 + \nu (d = a)$ and $c_2 = 13/6$, ν being defined in [13], where $C^u_{1,2}$ are unknown constants, and

$$(20)\quad f_1 = kb,\ p_1 = M_+(k)/\sqrt{b},\ u_1^\pm = U_\pm(\pm k)/b,$$

$$(21)\quad \xi(s) = \frac{\mathrm{e}^{\mathrm{i}(2ka - \pi/4)}}{\pi\sqrt{ka}} \Gamma_1[3/2, -2\mathrm{i}(s+k)a],$$

$$\eta(s_1, s_2) = \frac{\xi(s_1) - \xi(s_2)}{(s_1 - s_2)a}.$$

In (21), $\Gamma_1(\cdot,\cdot)$ is the generalized gamma function defined in [15].

Using (18) and (19), we can derive approximate expressions of (8a), which are valid for cavity depth $2a$ greater than about the wavelength. The unknowns $u_n^\pm$ for $n = 1, 2, 3, \cdots, N$ and $C^u_{1,2}$ are determined by solving an appropriate matrix equation numerically [12]. We have verified that the choice $N \geq 2kb/\pi$ provides sufficiently accurate results. Approximate expressions of (8b) are derived following the same procedure as above. The scattered field in real space for $|y| > b$ is evaluated asymptotically by taking the inverse Fourier transform of (4) and applying the saddle point method.

III. A CAVITY WITH CIRCULAR CROSS SECTION : THE RIEMANN-HILBERT PROBLEM APPROACH

We now consider a 2-D loaded cavity illuminated by an E-polarized plane wave, as shown in Figure 2, where the cavity wall is infinitely thin and perfectly conducting while the ring-shaped loading has the relative material constants ε_r, μ_r. Let the total electric field be defined by the same expression as in the previous section (see (1) and (2)) except that we set $E_z^i \equiv 0$ for $r < a$. The scattered field E_z can be expanded as

$$(22)\quad E_z(r,\varphi) = \sum_{n=-\infty}^{\infty} f_n(r)\, \mathrm{e}^{\mathrm{i}n\varphi},$$

in cylindrical coordinates using the Bessel and Hankel functions, where

$$(23)\quad f_n(r) = \begin{cases} A_n H_n^{(1)}(kr),\ r > a, \\ B_n J_n(kr) + C_n H_n^{(1)}(kr),\ d < r < a, \\ D_n J_n(k'r) + E_n H_n^{(1)}(k'r),\ c < r < d, \\ F_n J_n(kr),\ r < c. \end{cases}$$

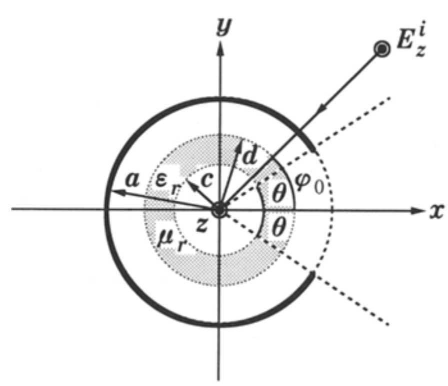

FIG. 2. — Geometry of the circular cavity.

Géométrie de la cavité circulaire.

Applying the boundary conditions for E_z^t and $\partial E_z^t/\partial r$ at $r = c, d$ to eliminate B_n, C_n, D_n, E_n, F_n in (23) and then taking into account the boundary condition at $r = a$, we arrive at the dual series equations (DSE) :

(24a) $$\sum_{n=-\infty}^{\infty} x_n\, e^{in\varphi} = 0, \;\; \theta < |\varphi| \le \pi,$$

(24b) $$\sum_{n=-\infty}^{\infty} \frac{x_n \xi_n [H_n^{(1)}(ka)]^{-1} e^{in\varphi}}{\xi_n J_n(ka) + \zeta_n H_n^{(1)}(ka)} = \sum_{n=-\infty}^{\infty} \frac{(-i)^n e^{in(\varphi-\varphi_0)}}{H_n^{(1)}(ka)}, \;\; |\varphi| < \theta,$$

where

(25) $$x_n = A_n H_n^{(1)}(ka) + (-i)^n J_n(ka) e^{-in\varphi_0}, \;\; \eta = \sqrt{\varepsilon_r/\mu_r},$$

(26) $$\xi_n = \gamma_n H_n^{(1)\prime}(kd) - \delta_n H_n^{(1)}(kd), \quad \zeta_n = \delta_n J_n(kd) - \gamma_n J_n'(kd),$$

(27) $$\gamma_n = \alpha_n J_n(k'd) + \beta_n H_n^{(1)}(k'd), \quad \delta_n = \eta[\alpha_n J_n'(k'd) + \beta_n H_n^{(1)\prime}(k'd)],$$

(28a) $$\alpha_n = \eta J_n(kc) H_n^{(1)\prime}(k'c) - H_n^{(1)}(k'c) J_n'(kc),$$

(28b) $$\beta_n = J_n(k'c) J_n'(kc) - \eta J_n(kc) J_n'(k'c).$$

In the above, the prime on $H_n^{(1)}(\cdot)$ and $J_n(\cdot)$ implies differentiation with respect to the argument. Introducing the function of a complex variable $z = |z| e^{i \arg z}$ as $X(z) = \sum_{n=1}^{\infty} n x_n z^{\mathrm{sgn}(1-|z|)n}$, the DSE can be formulated in terms of the Riemann-Hilbert functional equation satisfied by the limiting values of $X(z)$ on the unit circle $|z| = 1$. This equation can be solved exactly based on the theory of Cauchy's integrals [9] resulting in the matrix equation of the Fredholm second kind :

(29) $$x_m = \sum_{n=-\infty}^{\infty} K_{mn} x_n + L_m, \;\; m = 0, \pm 1, \pm 2, \cdots,$$

where

(30) $$K_{mn} = P_{mn} T_{mn}, \quad L_m = -(-i)^m e^{-im\varphi_0} [H_m^{(1)}(ka)]^{-1} + \sum_{n=-\infty}^{\infty} l_{mn} T_{mn},$$

(31a) $$P_{mn} = \frac{|n| J_n(ka) H_n^{(1)}(ka)}{J_m(ka) H_m^{(1)}(ka)} + \frac{i}{\pi} \frac{\xi_n J_n(ka) [J_m(ka) H_m^{(1)}(ka)]^{-1}}{\xi_n J_n(ka) + \zeta_n H_n^{(1)}(ka)},$$

(31b) $$l_{mn} = \frac{|n|(-i)^n J_n(ka) e^{-in\varphi_0}}{J_m(ka) H_m^{(1)}(ka)} + \frac{i^{1-n} \xi_n e^{-in\theta_0} [J_m(ka) H_m^{(1)}(ka)]^{-1}}{\pi[\xi_n J_n(ka) + \zeta_n H_n^{(1)}(ka)]},$$

(32) $$T_{mn} = \begin{cases} Q_{mn}(\cos\theta), \; m \ne 0, \\ Q_{n0}(\cos\theta), \; m = 0, \; n \ne 0, \\ -\ln[(1+\cos\theta)/2], \; m = n = 0, \end{cases}$$

and $Q_{mn}(\cdot)$ in (32) is given in [14] in terms of the Legendre polynomials.

We can show by taking into account the asymptotic behavior of K_{mn} for $|m|$, $|n| \to \infty$, together with the Fredholm theorems, that the unique solution of (29) exists and is approximated by the solution of a truncated matrix equation with any desired accuracy. Practically, after separating the matrix into even and odd parts, $|k'|a + 10$ equations are sufficient to obtain the far field quantities within the 0.1% accuracy. Unlike the conventional MM solutions, no numerical integrations are required for computing the matrix elements and hence, the present solution is efficient in a computational sense.

IV. NUMERICAL RESULTS AND DISCUSSION

We shall now present numerical examples on the RCS to discuss the far field scattering characteristics of rectangular and circular cavities for both E and H polarizations. In order to have a better ground for comparison, we take a square-shape cavity ($a = b$ in Figure 1) and a three-quarter circular cavity ($\theta = 45°$ in Figure 2) with the same material constants $\varepsilon_r = 2.5 + i1.25$, $\mu_r = 1.6 + i0.8$. For rectangular cavities, the material layer is located either on the aperture ($d = a$) or on the endplate ($c = -a$), whereas the loading for circular cavities is such that the material layer is lined along the interior cavity surface and covers the aperture ($d = a$). The material layer thickness $t (\equiv d - c)$ has been chosen as 0.2 a for rectangular cavities and 0.1 a for circular cavities. The results for empty cavities have also been added for investigating the effect of material loading.

Figures 3 and 4 show the frequency dependences of the monostatic RCS for rectangular and circular cavities, respectively, where the incidence angle is $\varphi_0 = 10°$ for both geometries. In the figures, the results of closed rectangular and circular cylinders are also included for comparison. It is seen from Figures 3 and 4 that the empty circular cavity exhibits stronger resonances than the rectangular one. This is perhaps due to the whispering-gallery behavior of higher order natural modes in the circular cavity, which does not appear in the rectangular case. We also observe that the absorbing layer loading

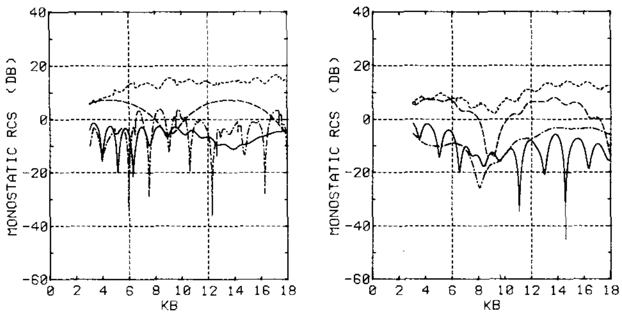

a b

FIG. 3. — Monostatic RCS (dB) versus normalized frequency kb of a rectangular cavity with $\varphi_0 = 10°$, $a/b = 1.0$, $t/a = 0.2$ ($t = d - c$).
– – – – : closed ; - - - - : empty ; —— : $d = a$; – - – - – : $c = -a$.
(a) E polarization. (b) H polarization.

RCS monostatique (dB) rapportée à la fréquence normalisée kb pour une cavité rectangulaire avec $\varphi_0 = 10°$, $a/b = 1.0$, $t/a = 0.2$ ($t = d - c$).
– – – – : fermé ; - - - - : vide ; —— : $d = a$ *; – - – - – :* $c = -a$.
(a) Polarisation E. (b) Polarisation H.

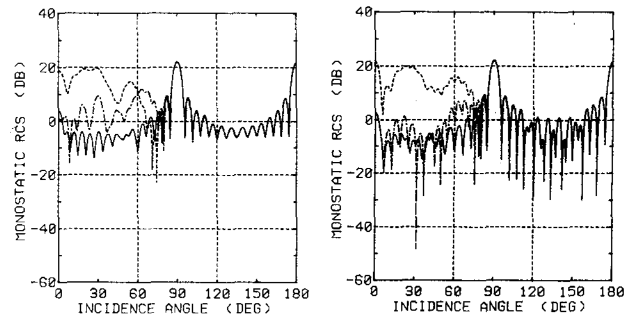

a b

FIG. 5. — Monostatic RCS (dB) versus incidence angle φ_0 of a rectangular cavity with $kb = 15.7$, $a/b = 1.0$, $t/a = 0.2$ ($t = d - c$).
- - - - : empty ; —— : $d = a$; – - – - – : $c = -a$.
(a) E polarization. (b) H polarization.

RCS monostatique (dB) rapportée à un angle d'incidence φ_0 *pour une cavité rectangulaire avec* $kb = 15.7$, $a/b = 1.0$, $t/a = 0.2$ ($t = d - c$).
- - - - : vide ; —— : $d = a$ *; – - – - – :* $c = -a$.
(a) Polarisation E. (b) Polarisation H.

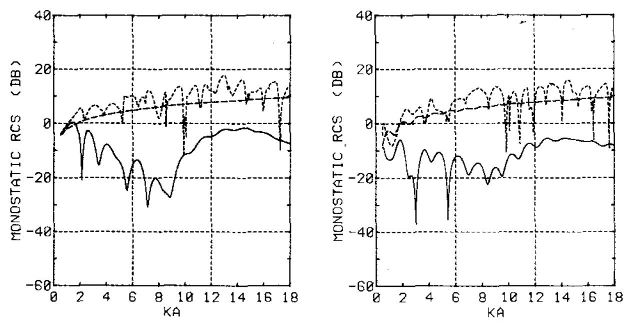

a b

FIG. 4. — Monostatic RCS (dB) versus normalized frequency ka of a circular cavity with $\varphi_0 = 10°$, $\theta = 45°$, $t/a = 0.1$ ($t = d - c$).
– – – – : closed ; - - - - : empty ; —— : $d = a$.
(a) E polarization. (b) H polarization.

RCS monostatique (dB) rapportée à la fréquence normalisée ka pour une cavité circulaire avec $\varphi_0 = 10°$, $\theta = 45°$, $t/a = 0.1$ ($t = d - c$).
– – – – : fermé ; - - - - : vide ; —— : $d = a$.
(a) Polarisation E. (b) Polarisation H.

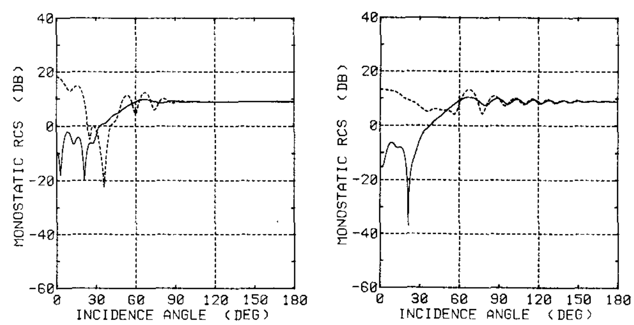

a b

FIG. 6. — Monostatic RCS (dB) versus incidence angle φ_0 of a circular cavity with $ka = 15.7$, $\theta = 45°$, $t/a = 0.1$ ($t = d - c$).
- - - - : empty ; —— : $d = a$.
(a) E polarization. (b) H polarization.

RCS monostatique (dB) rapportée à un angle d'incidence φ_0 *pour une cavité circulaire avec* $ka = 15.7$, $\theta = 45°$, $t/a = 0.1$ ($t = d - c$).
- - - - : vide ; —— : $d = a$.
(a) Polarisation E. (b) Polarisation H.

leads to the reduction of the average RCS level for both geometries, and suppresses the resonances at higher frequencies for circular cavities. In Figures 5 and 6, the monostatic RCS is presented as a function of incidence angle for rectangular and circular cavities, respectively. To enable comparison between the two different geometries, normalized dimensions of the cavities are taken as $ka = kb = 15.7$. It is observed by comparing the results for empty and loaded cavities that, when the cavity aperture is in the illuminated region against the incident field, the RCS is reduced for loaded cavities. This reduction can be seen especially over $0° < \varphi_0 < 30°$ and is significant in the H polarization. Shown in Figures 7 and 8 are the bistatic RCS results as a function of observation angle for rectangular and circular cavities, respectively, where the incidence angle is fixed as $\varphi_0 = 10°$ and the cavity dimensions are the same as in Figures 5 and 6. From the results presented in the figures, we see the shadow lobes along the forward scattering direction $\varphi = -170°$, as expected. The RCS reduction is again observed for loaded cavities over the region where the cavity aperture is visible from the observation point, and it is noticeable for $|\varphi| < 60°$ and in the H-polarized case.

ACKNOWLEDGMENTS

The authors would like to thank Professor Ayhan Altintas for many helpful discussions. They are also indebted to Ms. Dilek Çolak and Mr. Shoichi Koshikawa for assisting in the preparation of the manuscript. This work was supported in part by the 1992 Chuo University Special Research Grant and by the Matsumae International Foundation.

Manuscrit reçu le 26 septembre 1994.

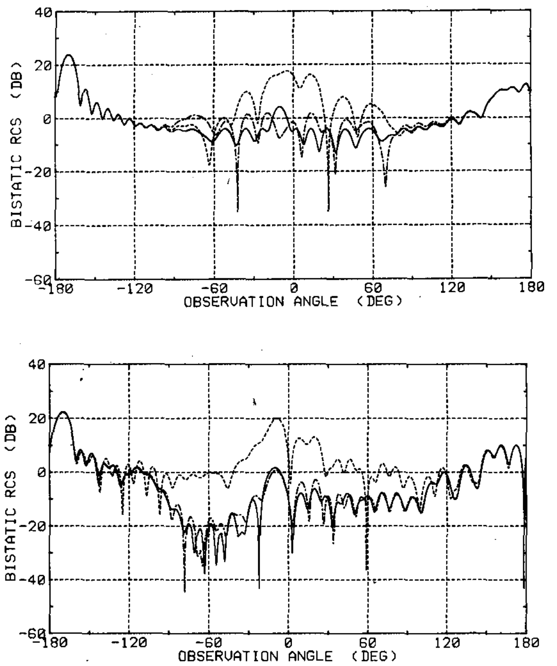

a

b

FIG. 7. — Bistatic RCS (dB) versus observation angle φ of a rectangular cavity with $\varphi_0 = 10°$, $kb = 15.7$, $a/b = 1.0$, $t/a = 0.2$ ($t = d - c$).
- - - - : empty ; —— : $d = a$; – - – - – : $c = -a$.
(a) E polarization. (b) H polarization.

RCS bistatique (dB) rapportée à un angle d'observation φ pour une cavité rectangulaire avec $\varphi_0 = 10°$, $kb = 15.7$, $a/b = 1.0$, $t/a = 0.2$ ($t = d - c$).
- - - - : vide ; —— : $d = a$; – - – - – : $c = -a$.
(a) Polarisation E. (b) Polarisation H.

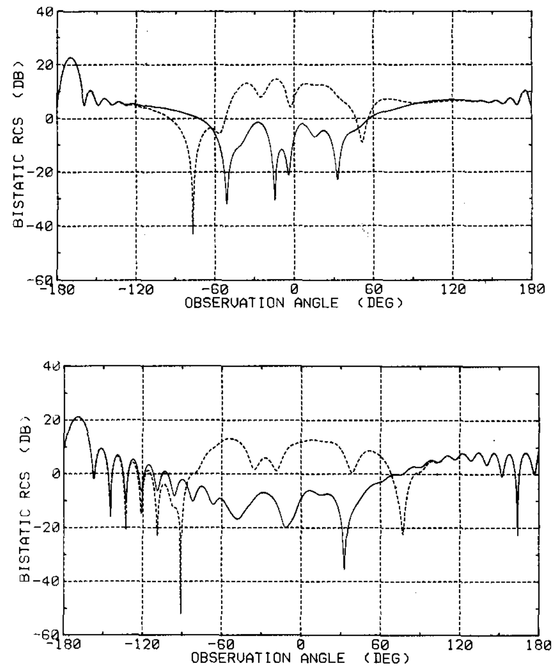

a

b

FIG. 8. — Bistatic RCS (dB) versus observation angle φ of a circular cavity with $\varphi_0 = 10°$, $ka = 15.7$, $\theta = 45°$, $t/a = 0.1$ ($t = d - c$).
- - - - : empty ; —— : $d = a$.
(a) E polarization. (b) H polarization.

RCS bistatique (dB) rapportée à un angle d'observation φ pour une cavité circulaire avec $\varphi_0 = 10°$, $ka = 15.7$, $\theta = 45°$, $t/a = 0.1$ ($t = d - c$).
- - - - : vide ; —— : $d = a$.
(a) Polarisation E. (b) Polarisation H.

REFERENCES

[1] LEE (C. S.), LEE (S.-W.). RCS of a coated circular waveguide terminated by a perfect conductor. *IEEE Trans. AP* (1987), **35**, n° 4, pp. 391-398.

[2] ALTINTAS (A.), PATHAK (P. H.), LIANG (M. C.). A selective modal scheme for the analysis of EM coupling into or radiation from large open-ended waveguides. *IEEE Trans. AP* (1988), **36**, n° 1, pp. 84-96.

[3] MAUTZ (J. R.), HARRINGTON (R. F.). EM penetration into a conducting circular cylinder through a narrow slot, TM case. *J. Electromagn. Waves Appl.* (1988), **2**, n° 3/4, pp. 269-293.

[4] LING (H.), CHOU (R.-C.), LEE (S.-W.). Shooting and bouncing rays : calculating the RCS of an arbitrary shaped cavity. *IEEE Trans. AP* (1989), **37**, n° 2, pp. 194-205.

[5] PATHAK (P. H.), BURKHOLDER (R. J.). Modal, ray, and beam techniques for analyzing the EM scattering by open-ended waveguide cavities. *IEEE Trans. AP* (1989), **37**, n° 5, pp. 635-647.

[6] FELSEN (L. B.), VECCHI (G.). Wave scattering from slit coupled cylindrical cavities with interior loading : Part II - resonant mode expansion. *IEEE Trans. AP* (1991), **39**, n° 8, pp. 1085-1097.

[7] GOGGANS (P. M.), SHUMPERT (T. H.). Backscatter RCS for TE and TM excitations of dielectric-filled cavity-backed apertures in two-dimensional bodies. *IEEE Trans. AP* (1991), **39**, n° 8, pp. 1224-1227.

[8] NOBLE (B.). Methods based on the Wiener-Hopf technique for the solution of partial differential equations. *Pergamon* (1958).

[9] GAKHOV (F. D.). Boundary value problems. *Pergamon* (1966).

[10] NOSICH (A. I.). Green's function-dual series approach in wave scattering by combined resonant scatterers, *in* Analytical and numerical methods in electromagnetic wave theory, Hashimoto (M.), Idemen (M.), Tretyakov (O. A.), Eds. *Science House* (1993), Chap. 9.

[11] ZIOLKOWSKI (R. W.), GRANT (J. B.). Scattering from cavity-backed apertures : the generalized dual series solution of the concentrically loaded *E*-pol slit cylinder problem. *IEEE Trans. AP* (1987), **35**, n° 5, pp. 504-528.

[12] KOBAYASHI (K.), SAWAI (A.). Plane wave diffraction by an open-ended parallel plate waveguide cavity. *J. Electromagn. Waves Appl.* (1992), **6**, n° 4, pp. 475-512.

[13] KOBAYASHI (K.), KOSHIKAWA (S.), SAWAI (A.). Diffraction by a parallel-plate waveguide cavity with dielectric/ferrite loading : part I - the case of *E* polarization. *In* Progress in electromagnetics research, Pier 8, KONG (J. A.), Ed. *EMW Publishing* (1994), Chap. IX.

[14] ÇOLAK (D.), NOSICH (A. I), ALTINTAS (A.). Radar cross-section study of cylindrical cavity-backed apertures with outer or inner material coating : the case of *E*-polarization. *IEEE Trans. AP* (1993), **41**, n° 11, pp. 1551-1559.

[15] KOBAYASHI (K.). On generalized Gamma functions occurring in diffraction theory. *J. Phys. Soc. Jap.* (1991), **60**, n° 5, pp. 1501-1512.

BIOGRAPHIES

Kazuya KOBAYASHI was born in 1955. He received the Ph.D. degree in electrical engineering from Waseda University, Tokyo, Japan, in 1982. Since 1982 he has been with the Department of Electrical and Electronic Engineering, Chuo University, Tokyo, Japan, where he is currently a Professor.

Alexander I. NOSICH was born in 1953. He received the Ph.D. and D.Sc. degrees in radio physics from Kharkov University, Ukraine, in 1979 and 1990, respectively. Since 1978, he has been with the Electronics Department, Institute of Radiophysics and Electronics, Ukrainian Academy of Sciences, Kharkov, Ukraine, where he is currently a Leading Scientist.